Int. J. Nanosci. Nanotechnol., Vol. 19, No. 2, June 2023, pp. 65-76
DOI: 10.22034/ijnn.2023.555186.2219

A Novel Co-Precipitation Route for the Synthesis of Pure and Ni-Doped CuO Nanoparticles: Effect of Doping on Structural, Optical, and Electrical Properties

Manauwar Ali Ansari[1,*] and Nusrat Jahan[2]

[1]Hevesy György PhD School of Chemistry, Eötvös Loránd University,
Pázmány Péter sétány 1/A, H-1117, Budapest, Hungary
[2]School of Science, J S University, Shikohabad, India

(*) Corresponding author: maansarivce@gmail.com
(Received: 05 June 2022 and Accepted: 28 February 2023)

Abstract

A novel route for the synthesis of pure and nickel (Ni) doped copper oxide (CuO) nanoparticles via a simple co-precipitation process has been presented. The effect of the concentration of the dopant Ni (0, 2, and 4 mol %) on its properties has been carefully investigated. It has been reported that Ni doping is successfully achieved through the synthesis route. The structure and morphology were analyzed by using X-ray diffraction, Fourier transform infrared spectroscopy, and field emission scanning electron microscopy. X-ray diffraction analysis proved that prepared nanoparticles are highly pure and crystalline having a monoclinic structure and the crystallite size increases (13 nm to 17 nm) with Ni doping. Fourier transform infrared spectrum show successful Ni doping in the CuO system. Optical properties were investigated using UV-vis spectroscopy and the calculated band gap energies are 4.64 and 4.71 eV for pure and doped CuO, respectively. Electrical properties (dielectric constant (ε'), dielectric loss (tan δ), and AC conductivity (σ_{ac}) were studied using room temperature impedance spectroscopy. Energy dispersive X-ray spectrum of undoped and Ni-doped CuO to confirm the prepared sample composition has also been presented and discussed.

Keywords: *Co-precipitation, Copper oxide, Electrical property, Nanoparticles, Nickel doping, Optical property.*

1. INRODUCTION

Nanostructured materials are of great interest in current material research from basic as well as applied research point of view due to their dramatic change in properties in the nanometre range [1]. The oxides of transition metals or TMOs such as Fe_3O_4, SnO_2, TiO_2, ZnO, etc. are a significant group of semiconductors, which have unique material properties in contrast to their bulk phase, making it broad applications in different areas [2-12].

Among the TMOs, cupric oxide (CuO) is especially fascinating because of having a variety of chemo-physical properties which makes it applicable in many areas, such as conversion of energy, optoelectronic devices, and gas sensing [13], catalysts [14], high-Tc superconductors [15], etc. It also shows antibacterial and cancer-fighting features [16-19]. CuO is a p-group narrow band gap semiconductor which is useful in photoconductive and photo-thermal uses [20]. In addition to these, a large dielectric constant of CuO opens exciting possibilities in microelectronics [21-23].

Hitherto, several preparation routes have been established to produce CuO nano-particles of various shapes and sizes such as sol-gel [24, 25], chemical method [26], hydro-thermal [27], thermal decomposition [28], sono-chemical [29], microwave irradiation [30] and quick- precipitation [31, 32], etc. Among these processes, the

co-precipitation method has gained great interest in industries due to the facile way of synthesis, low temperature and energy, cost- effective approach for large-scale production and good yield.

As we already know, the nanoparticles' physical properties are mainly determined by their microstructure (crystals grain boundaries, crystal defects as well as surface morphology). Therefore, for a well understanding of materials' size-dependent physical properties, it is significantly important to get the knowledge of the microstructure of CuO NPs. The structural, optical, and electrical characteristics of CuO NPs are of great topic of concern as it to be used as electrode materials, gas sensors, and for many devices and systems. Furthermore, by doping with foreign metal ions we can tailor the chemo-physical properties of nanomaterials.

In the literature, several authors have observed the changes associated with CuO doping with transition metals, like Fe [33-36], Mn [37, 38], Ag, Cd, Zn, and Ti [39]. There are few studies on Ni-doped nanophase CuO was reported [40-44]. Meneses et al. prepared Ni-doped CuO NPs through the co-precipitation method followed by high-temperature annealing at 800 ^{o}C for 5h and reported the magnetic properties [36]. Basith et al. synthesized Ni-doped CuO by microwave-assisted combustion route and reported an enhancement in the band gap from 3.9 eV to 4.3 eV by increasing the Ni content. They also reported room temperature-ferromagnetism with a saturation magnetization (Ms) of 1.31 x 10^{-3} emu/g at 2.0 wt% of Ni [40]. Al-Amri et al. prepared Ni-doped CuO NPs using a sol-gel combustion method and an obvious increase of band gap has been estimated [41]. Lakshmi et al. prepared Nickel doped CuO- NPs by hydrothermal method and catalytic reduction of Triethyl phosphate (TEP) monitored and proved using UV-vis spectrophotometer [42]. Thangamani et al. synthesized Nickel substituted CuO NPs by microwave irradiation technique and studied and confirmed the ferromagnetic behavior of the NPs at room temperature [43]. Arunachalam et al. prepared Ni-CuO nanocomposite by the co-precipitation process and studied the electro-oxidation of methanol by varying the factors such as catalyst quantity (Ni-doped CuO) and the concentration of methanol solution [44]. The aim of this work is to observe the effect of Ni doping on the opto-electric property of CuO NPs. Also, we understand that up to now there is no work published on electrical properties such as dielectric constant, loss factor, and AC conductivity of Ni-doped copper oxide nanoparticles synthesized using co-precipitation route.

In our present study, we prepared pure and Ni-doped CuO nanoparticles through a novel, cost- effective, co-precipitation method. Ni was added as a dopant in two different mole % viz. 2 and 4. The influence of Ni doping on the structural, optical, and electrical properties including dielectric constant, dielectric loss, and AC conductivity of CuO nanocrystals is first time reported using X-ray diffraction (XRD), Fourier transform infrared spectroscopy (FTIR), field emission scanning electron microscopy (FESEM), energy dispersive X-ray analysis (EDS), UV-Vis, and impedance spectroscopy.

2. MATERIALS AND METHOD

2.1. Materials and Synthesis Process

All the reagents utilized for this work were of analytical quality, obtained from Merck, India, and were used as purchased without further purification. Copper nitrate ($Cu(NO_3)_2 \cdot 3H_2O$), 99.5%), and nickel nitrate ($Ni(NO_3)_2 \cdot 3H_2O$), 99.5%) were used as precursors and sodium bicarbonate ($NaHCO_3$) as a fuel for this reaction.

CuO NPs were prepared using a chemical co-precipitation method. The schematic of the synthesis process is presented in Figure 1. In a common synthesis, 0.5 M of tri-hydrated copper nitrate was mixed in 100 ml of de-ionized water (H_2O) through magnetic stirring for

approximately 30 min until the copper nitrate dissolved completely. Sodium bicarbonate solution was then added drop by drop into the copper nitrate solution, under constant stirring. At this stage tri-hydrated nickel nitrate solution can be added for doping. After continuous stirring for approximately 2 hours the reaction mixture forms completely having sky blue colour. The formed mixture is then kept for 12 hours insuring that constituent particles are completely get precipitated. The precipitated mixture was then washed throughly and centrifuged a number of times using distilled water to remove native impurities from it. Finally, the precipitated mixture paste dried under the air at 100 °C for 24 hours and then calcined at 400-500 °C for 4 hours, ensuring that cupric carbonate ($Cu_2(OH)_2CO_3$) was completely converted into CuO. Although, the black colour is indicative of the calcined material is CuO rather than Cu_2O (red colour). The following are examples of probable chemical reactions [45]:

$$2Cu(NO_3)_2\ (aq.) + 4NaHCO_3\ (aq.) \rightarrow 4NaNO_3\ (aq.) + Cu_2(OH)_2CO_3\ (aq.) + H_2O + 3CO_2$$

$$Cu_2(OH)_2CO_3 \rightarrow 2CuO + H_2O\uparrow + CO_2\uparrow \text{ (calcination)}$$

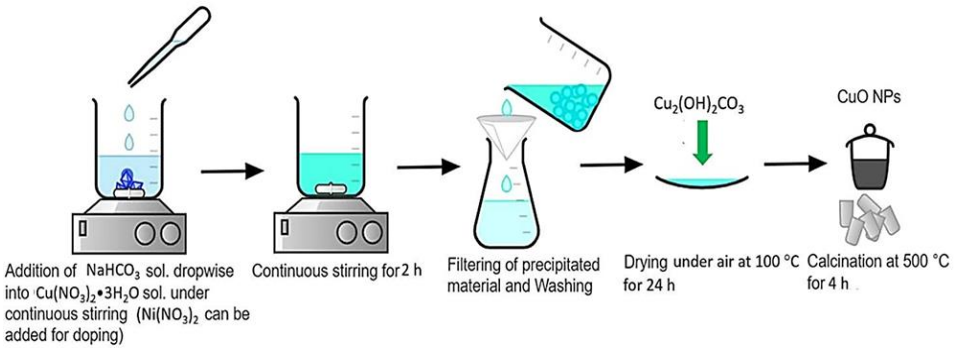

Figure 1. *Schematic of synthesis procedure of pure and Ni-doped CuO nanoparticles.*

2.2. Characterization

XRD (X-ray diffractometer, Rigaku-Miniflex, Japan) method was used to characterise structural features such as phase and crystallinity of as-synthesised samples using Cu-Kα radiations (λ = 1.5406 Å) in the 2θ range 20°- 80°. Morphology of the sample was observed by FEI FE-SEM (field emission scanning electron microscopy). The energy dispersive X-ray spectrum (EDS) was taken to ascertain elemental composition of the prepared sample. PerkinElmer, USA, FTIR (Fourier transforms infrared) spectroscopy was used in transmission mode to determine the chemical composition of powderform samples in the wavenumber range 400–4000 cm^{-1}. PerkinElmer, UV-visible was employed to acquire the room temperature- absorbance spectra of material in the wavelength range 200 nm-800 nm. In order to perform measurement of electrical properties, the pellet samples were prepared, metallizing both faces with highly pure (99.99 %) silver using thermal evaporation. Keithley, USA, 3330 LCZ meter type room temperature-dielectric spectroscopy was employed in the range of 0.1 MHz-10 MHz to analyse the electrical properties (dielectric constant, dielectric loss, and AC conductivity).

3. RESULTS AND DISCUSSION

3.1. Structural and Morphological Properties

3.1.1. X-ray Diffraction

XRD patterns of pure and Ni-doped CuO samples are taken and presented in Figure 2. In the obtained XRD patterns all peaks

correspond to planes (110), (002), (111), (202), (020), (202), (113), (311), and (113) are labeled to the monoclinic phase of CuO that was verified with standard data (JCPDS card No. 05-0661). The characteristics peaks of the pure CuO NPs monoclinic phase are found at 2θ = 35.65 and 38.84 correspond to planes (002) and (111), respectively. The XRD spectra contain no impurities like Cu_2O, Ni oxides, and Ni metal, which shows the purity and single-phase of the NPs prepared. Also, peak sharpness clearly suggests a single phase of highly crystalline Ni-doped CuO NPs formation. A gradual shift of main peaks of doped samples towards lower 2θ values was detected as compared to pure CuO, which arose because of crystal lattice strain due to the difference in Cu^{2+} and Ni^{2+} ionic radii [46].

The increase of lattice parameter and hence average crystallite size with Ni content is due to enhancement in the concentration of molecules at the crystal surface [40, 41]. The average crystallite size (D) of the as prepared samples was calculated using Scherrer's equation [47].

$$D = \frac{K\lambda}{\beta \cos\theta} \quad (1)$$

Where K is the shape factor (0.90), λ is the wavelength of Cu-Kα radiation, β is the full-width at half maximum (FWHM), and θ is the diffraction angle. The mean crystallite size of pure CuO NPs is calculated to be 13.37 nm. By inclusion of Ni^{2+} content of wt. % 2 to 4 average crystallite size increases from 14.31 nm to 17.07 nm.

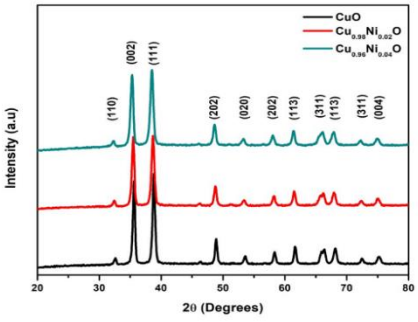

Figure 2. *XRD patterns of as-synthesized pure and Ni-doped CuO nanoparticles.*

3.1.2. SEM and EDS

X SEM images for pure and 4% Ni-doped samples are shown in Figure 3(a) and 3(b), respectively. The figure shows pure CuO has some rounded cubic shape and 4% Ni-doped CuO has some rod shape morphology as given in the enhanced part of the Figure 3(b). The crystallite size as seen in the SEM images in accordance with the results of XRD analysis. Figure 4(a) and 4(b) shows the EDS spectrum, collected from the average scanned area of pure and 4% Ni-doped CuO nanoparticles. EDS study showed strong peaks of only Cu and O elements for the pure sample and Cu, O and, Ni elements for Ni-doped samples, whereas no additional peaks are found, which indicates that the as-prepared nano powder is freed from impurities that emerging from the initial precursors, like sodium, nitrogen, and carbon, etc. Thus, doping of the Ni^{2+} is successfully done in the Cu sites. The atomic percentage of sample's compositional elements (Ni, Cu and O) present in undoped CuO and 4% Ni-doped CuO NPs are presented in Table 1. The calculated ratio of atomic percentage of Ni and Cu was found to be 0.0395 (~4%) in 4% Ni- doped CuO NPs. Hence, EDS spectra correspond to the experimental results [27, 40].

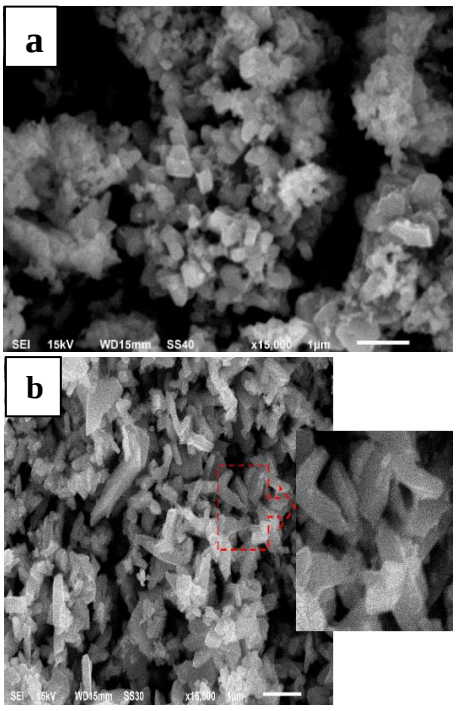

Figure 3. *SEM images of (a) Pure (b) 4% Ni-doped CuO nanoparticles, enhanced part showing nanorods shaped nanoparticles.*

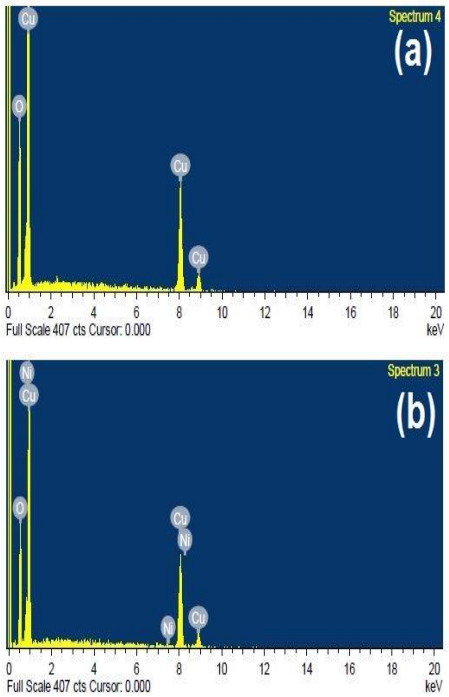

Figure 4. *EDS spectra of (a) pure and (b) 4 % Ni-doped CuO nanoparticles.*

Table 1. *The atomic percentage ratio of Cu, Ni and O in CuO and Ni-doped CuO nanoparticles.*

Sample ratio	Atomic percentage (%) of the elements			
	Cu	O	Ni	Ratio of atomic perc. (Ni/Cu)
CuO	32.52	67.48	--	--
$Ni_{0.04}Cu_{0.96}O$	36.67	61.88	1.45	0.0395

3.1.3. Fourier Transform Infrared Spectroscopy

FTIR spectroscopy is an analysis technique, used for determining the vibrational frequency band of molecules and to analyze the surface nature of nanophase CuO. Figure 5(a) and 5(b) show FTIR spectra for pure and Ni-doped CuO nanoparticles. The broad absorption band centered at 3425 cm^{-1} associated with the stretching vibration of the O-H group which is maybe because of the water molecules absorption by sample. The absorption peak near 2928 cm^{-1} is due to C-H `stretching mode and the peak arose at 1023 cm^{-1} is possibly due to the O-H deformation band. It is also clear from Figure 5 that all samples show bands in region 400 cm^{-1}-600 cm^{-1}. The strong band at 535 cm^{-1} and 596 cm^{-1} are in accord with the vibration stretching of the Cu–O bond. The obtained frequency bands show good agreement to the previously published literature [17, 27, 42, 43, 47]. Moreover, no frequency band has been observed corresponding to the secondary phase i.e., cuprous oxide (Cu_2O) in the material system which confirms the purity and successful formation of single-phase Ni-CuO NPs [48, 49]. Also, it is observed from the spectra that IR analysis depends on crystallite size, as Ni concentration increases, the intensity, and bandwidth of FTIR peaks increases. Moreover, the broadening of the IR absorption band could be the consequence of alterations within CuO lattice's microstructure, lattice parameter changes, or variations in the system's free electron concentration. It is evident that all the char-

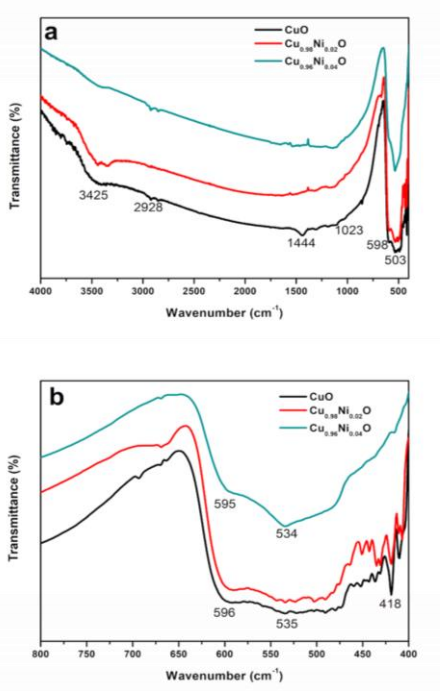

Figure 5. *(a) FTIR spectra for pure and Ni-doped CuO nanoparticles (b) zoomed*

view of spectra between region 400 cm^{-1} to 800 cm^{-1}.

-acteristic peaks have a slight shift, which may be explained by the variation in bond length that results from the replacement of Cu ions with Ni ions. This supports the successful formation of Ni-doped CuO [42, 43].

3.2. Optical Properties

3.2.1. UV-vis Spectroscopy

UV-vis absorption spectra of pure and Ni-doped CuO have recorded in the wavelength range of 200 nm-800 nm, as represented in Figure 6(a). The figure shows the three samples viz 0, 2, and 4 % doping the respective absorption peaks at roughly 267, 265, and 263 nm. The optical band gap (E_g) of as prepared samples was calculated by the Tauc equation, which gives a relation among the incoming photon energy and the absorption coefficient of the semiconducting materials. Tauc's relation [50] can be written as.

$$(\alpha h\nu) = A\left(h\nu - E_g\right)^n \quad (2)$$

Where A is proportionality constant, α is the materials absorption coefficient, hυ is energy of incoming photon (h: plank constant and υ: photon frequency), E_g is the optical band gap energy, *n* is a mathematical exponent whose value strongly influenced by the existence of the electronic transitions that causes light absorption. In general, *n* is considered equals to 2 and 1/2 for indirect and direct band gap, respectively. The intercept of plot for a direct band gap transition provides E_g [25] as shown in Figure 6(b).

The calculated band gap energy for pure (0%) CuO is 4.64 eV, and it is 4.68 and 4.71 eV for 2% and 4%, respectively. Moreover, it is observed from Figure 6(a) that the blue shift i.e., shifting of the absorption peak of doped CuO NPs towards lower wavelength is a sign of the introduction of Ni^{2+} into the CuO lattice, known as quantum size effect [51]. Calculated E_g values show that it is decreased greatly as the Ni concentration is increased. It is also seen from Figure 6(b) that the bandgap energy is slightly increasing with the Ni doping percentage which was also reported by Basith et al. [40] and Al-Amri et al. [41] for Ni-doped CuO nanoparticles. The bandgap energy for pure CuO (0%) nanoparticles is 4.64 eV which is greater than its bulk phase i.e., 1.85 eV [52]. This increase in band gap energy is due to the renowned quantum size effect of nanophase material. This quantum size effect theory is applicable only when the crystallite size is comparable to and in the de- Broglie wavelength range of a charge carrier (i.e., in the nanometre range).

3.3. Electrical Properties

3.3.1. Dielectric Constant and Loss Factor

In this section, frequency dependent dielectric constant and loss factor is presented and discussed. Impedance spectroscopy or dielectric spectroscopy is employed to study the effects of frequency on the conduction processes in nanomaterials.

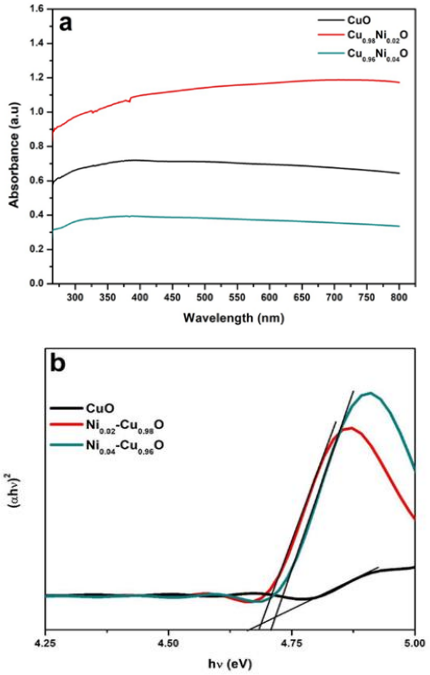

Figure 6. *(a) and (b) showing optical absorption spectra and the Tauc plot of*

pure and Ni-doped CuO nanoparticles, respectively.

The dielectric constant (ε) of a material can be expressed in the complex form as:

$$\varepsilon^* = \varepsilon' - j\varepsilon'' \quad (3)$$

where j is an imaginary number (satisfying $j^2 = -1$), ε' is real part of dielectric constant, responsible for the stored energy, calculated from the equation:

$$\varepsilon' = \frac{C_p d}{\varepsilon_o A} \quad (4)$$

and ε'' is imaginary part of dielectric constant, the cause of the energy loss which is expressed as:

$$tan\delta = \frac{\varepsilon''}{\varepsilon'} \quad (5)$$

Where C_p denotes capacitance of the sample, d denotes thickness of the pellet, A is the plane surface area of the pellet, ε_o denotes free space permittivity, and *tan δ* is called as loss factor.

To reach the conclusion on the dielectric feature components, we need to consider both the dielectric behavior as well as the polarizability together. In general, the sum of contributions due to various polarization mechanisms such as electronic, ionic, orientational, and space charge makes the overall polarizability of any material media. Each polarization mechanism has its own unique characteristic; their different type of contribution to overall polarizability is distinct from the others. Generally, a major proportion to dielectric constant comes from the charge carrier and orientational (dipolar) mechanism. The charge carrier mechanism involves partial recovery on discharge, leaving a finite polarization in media, while orientational (dipolar) involves the restoration of the zero residual polarization after discharge. (Figure 7a, and 7b)

The variation of real component of the dielectric constant with frequency (range 0.1 MHz-10 MHz) at room temperature for pure and 4% Ni-doped CuO is shown in Figure 8(a). It is clear from Figure 8(a) that the real part (ε') shows the general decreasing trend with the increase in frequency for both pure and doped samples. Also, at lower frequencies, the strong frequency dependence of ε' can be noted but further increase in frequency making ε' approaches a constant value.

This may be because the conductivity has the same root of origin via hopping between metal ions (Cu^{2+}, and Ni^{2+}). Generally, for pure CuO pellet, smooth (without peaks) decrease in the ε', confirming the overall relaxation is of non-Debye type character [53, 54]. This happened because, at lower frequencies, the hopping mechanism follo-

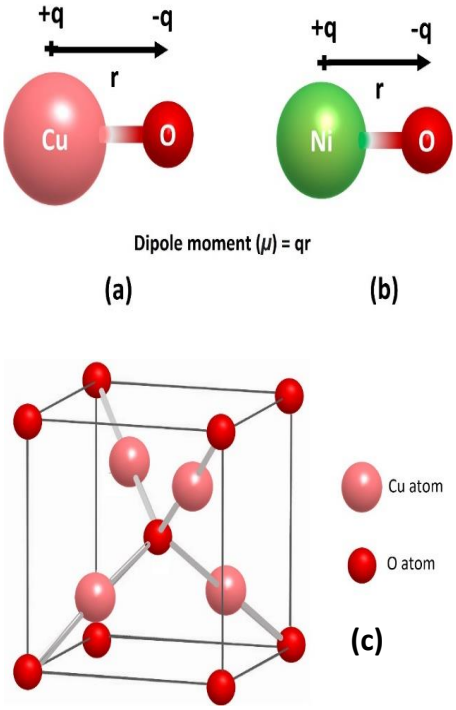

Figure 7. *Showing (a) the dipolar nature of a molecule of CuO, (b) the dipolar nature of a molecule of NiO, and (c) the atomic arrangement in the pure CuO crystal.*

-ws in accordance with the applied a. c. field, but when the frequency increased, the hopping stops following the frequent changes of the field and therefore, decreases because of unstable dipolar distribution and random orientation. The increment in ε' with Ni doping possibly

attributed to the enhanced electronegativity of Ni compared to Cu in the system. The electronegativity of Ni and Cu is 1.91 and 1.90 respectively on the Pauling scale.

The coordination of atoms in CuO is in such a way that there are four nearest-neighbor atoms of the different type for each atom. Each copper atom is connected to four almost coplanar oxygen atoms sited at the corners of a nearly rectangular parallelogram. The O atom is coordinated to four Cu atoms in the form, making a distorted tetrahedron (Figure 7c). In the case of pure CuO, electron density will exist near central oxygen atom in a distorted tetrahedron. Due to the shifting of electron density towards central oxygen atom bond angles are wide with a small value of resultant polarization. As Ni is introduced in the system electro-negativity of the Cu-Ni system slightly increases leading to the shift of electron density towards outer Cu-Ni atom, which in turn lowers the bond angles resulting the increase in resultant polarization and thereby increasing the dielectric constant up to 4%. As a result of this, the system's overall dipole moment falls abruptly decreasing the dielectric constant.

Dielectric losses generally involve the absorption current in the material. In polar dielectrics, a small component of electric energy is spent in the orientation of molecular dipoles along the direction of the applied external electric field to overcome the internal friction forces. In addition to this, a part of electric energy is also spent in the rotations of the molecular dipoles and other types of molecular relocation from one place to another, this also requires energy losses. In nanomaterial, defects, and interphase layers space charge formation inhomogeneities create an absorption current and hence dielectric loss [55].

Variation of dissipation factor or loss tangent (tan δ) with frequency at room temperature for different composition is shown in Figure 8(b). The peaking activity is shown by doped sample, which occurs when both the hopping frequency of metal ions and the frequency of the electric field become equal. It was seen that the peaking frequency moves towards higher frequency at 4% doping content. This indicates that the frequency of hopping related to metal ions (Cu^{+2}, and Ni^{+2}) increases with doping up to 4%. These observations correlate with the findings of ac conductivity well.

3.3.2. AC Conductivity

AC conductivity of CuO nanoparticles follows the frequency dependence as given by the power law according to the relation:

$$\sigma_{ac} = A f\omega^{n} \quad (6)$$

Where A is a constant, ω is the angular frequency, and n is the temperature and frequency, dependent exponent.

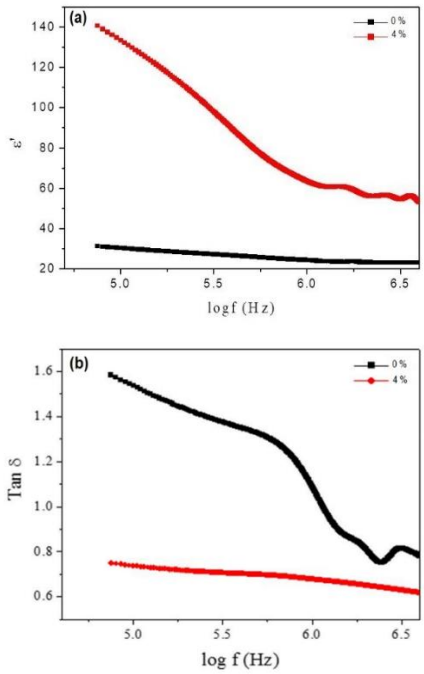

Figure 8. *Variation of (a) dielectric constant, and (b) loss factor with frequency of pure and 4% Ni-doped CuO nanoparticles.*

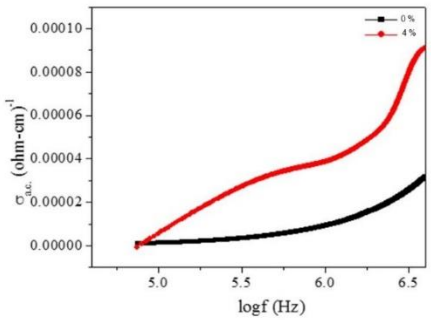

Figure 9. *Variation of AC conductivity with frequency of pure and 4% Ni-doped CuO.*

The overall conductivity of the material system is the contribution of both dc (frequency independent) and ac (frequency dependent) conductivities and can be represented as:

$$\sigma_{total} = \sigma_{dc} + \sigma_{ac} \quad (7)$$

To investigate the conduction mechanism involved a variation of exponent *n* with frequency and composition. The measurement of room temperature ac conductivity versus frequency was done and the plot for pure and 4% Ni-doped CuO was taken as shown in Figure 9. It's worth noting that the ac conductivity rises as the frequency increases for all the compositions. The enhancement in σ_{ac} correlates nicely with tanδ where the metal charge carriers hopping rate was found to rise with doping content [52, 53].

4. CONCLUSION

Ni-doped CuO nanoparticles were successfully synthesized using co-precipitation method without the need of any surfactant. XRD patterns confirmed the successful formation of pure and Ni-doped single-phase CuO nanoparticles. The average crystallite size of pure CuO NPs is found to be 13.37 nm. By inclusion of Ni^{+2} content of wt. % 2 to 4 average crystallite size increases from 14.31 nm to 17.07 nm. The calculated band gap energy for pure (0%) CuO is 4.64 eV and it was 4.68 and 4.71 eV for 2% and 4%, respectively. The band gap of the doped samples has widened. The real component of the dielectric constant shows the general decreasing trend with the rise in frequency for both pure and doped samples. At low frequencies, a strong frequency dependence of ε' was noted but further increase in frequency making ε' approaches a constant value, which happens because of the hopping mechanism. On doping with Ni^{+2}, the dielectric constant of CuO increased as compared to pure one which may be attributed to the enhanced electronegativity of Ni compared to Cu in the system. Dielectric loss curves show the peaking activity of all the samples, which occurs when both the metal ions hopping frequency and the frequency of the electric field become equal. It was seen that the peaking frequency moves towards higher frequency at 4% doping content. The ac conductivity rises with frequency for all the compositions.

Thus, the Ni doping in CuO improves the optical and electrical properties of the CuO nanoparticles. These results show that the synthesized Ni-doped CuO nanoparticles and nanostructures would be highly useful for optical and electrical material applications.

ACKNOWLEDGEMENT

Authors are thankful to the Department of Chemistry, Eötvös Loránd University, Hungary for valuable scientific and technical support.

CONFLICT OF INTEREST

The authors declare that they have no conflict of interest.

REFERENCES

1. Ansari, M. A., "Modelling of size-dependent thermodynamic properties of metallic nanocrystals based on modified Gibbs–Thomson equation", *Applied Physics A*, 127(5) (2021) 1-11.
2. Velayudhan Nair Girija, V., Vasu, S., "Synthesis and characterization of iron oxide nanoparticles by thermal decomposition method of iron (III) chelates", *International Journal of Nanoscience and Nanotechnology*, 15(1) (2019) 65-73.
3. Saravanan, S., Sivanandan, T., Ramalingam, G.,"Optical, Thermal and Magnetic Properties of Strontium Ferrite Nanoparticles", *International Journal of Nanoscience and Nanotechnology*, 18(4) (2022) 275-284.
4. Somdee, P., Ansari, M. A., Marossy, K.,"Thermo-mechanical properties of flexible and rigid polyurethane (PU)/Cu composites", *Polymer Composites*, 44(1) (2023) 401-412.
5. Sahu, K., Satpati, B., Mohapatra, S., "Facile fabrication of CuO nanosheets for photocatalytic applications", *Applied Physics A*, 127(5) (2021) 1-9.

6. Pirzad Ghias Abadi, S., Borhani Zarandi, M., Jahanbakhshi Zadeh, N., "Synthesis of NiO Nanoparticles: Effect of Method on Structural Properties of NiO Nanoparticles", *International Journal of Nanoscience and Nanotechnology*, 18(3) (2022) 187-195.
7. Devasia, J., Muniswamy, B., Mishra, M. K., "Investigation of ZnO Nanoparticles on In Vitro Cultures of Coffee (Coffea Arabica L.)", *International Journal of Nanoscience and Nanotechnology*, 16(4) (2020) 271-277.
8. Chandra Sekhar, D., Diwakar, B. S., Madhavi, N., "Silica Coated Magnetic Nanoparticles for Biological Applications *International Journal of Nanoscience and Nanotechnology*", 16(4) (2020) 209-217.
9. Ansari, M. A., Somdee, P., Marossy, K., "Synthesis of cross-linked polyurethane elastomers with the inclusion of polar-aromatic moieties (BA, PNBA and 3, 5-DNBA): Electrical and thermo- mechanical properties analysis", *Journal of Polymer Research*, 28(5) (2021) 1-11.
10. Hamzehzad, S., Keshipour, S., "TiO2/hydrophobic Cellulose Aerogel Nanocomposite as a New Photocatalyst for Oxidation of Alcohols and Ethylbenzene", *International Journal of Nanoscience and Nanotechnology*, 17(4) (2021) 231-238.
11. Peiravi, M. M., Ashabi, A., "Magneto Effects on Fe3O4 Nanoparticles through the Triangular and Rectangular Baffles on Thread Stretching Surface for Rotary Seals in Computer Hardware", *International Journal of Nanoscience and Nanotechnology*, 18(2) (2022) 143-156.
12. Soundararajan, S. P., Murugan, M., Mohanraj, K., Devendhiran, T., Balachandran, S., Balraj, B., Ho, M. S., "Characterization of CuO thin films and its Al/p-CuO/n-Si Schottky diodes fabricated via JNS pyrolysis technique", *Journal of Advanced Physics*, 7(2) (2018) 183-189.
13. Katti, V. R., Debnath, A. K., Muthe, K. P., Kaur, M., Dua, A. K., Gadkari, S. C., Sahni, V. C., "Mechanism of drifts in H2S sensing properties of SnO2: CuO composite thin film sensors prepared by thermal evaporation", *Sensors and Actuators B: Chemical*, 96(1-2) (2003) 245-252.
14. She, Y., Zheng, Q., Li, L., Zhan, Y., Chen, C., Zheng, Y., Lin, X., "Rare earth oxide modified CuO/CeO2 catalysts for the water–gas shift reaction", *international journal of hydrogen energy*, 34(21) (2009) 8929-8936.
15. Zheng, X. G., Xu, C. N., Tomokiyo, Y., Tanaka, E., Yamada, H., Soejima, Y., "Observation of charge stripes in cupric oxide", *Physical Review Letters*, 85(24) (2000) 5170.
16. Lakshmanan, S. P., Jostar, S. T., Arputhavalli, G. J., Jebasingh, S., Josephine, C. M. R., "Role of Green Synthesized CuO Nanoparticles of Trigonella Foenum- Graecum L. Leaves and their Impact on Structural, Optical and Antimicrobial Activity", *International Journal of Nanoscience and Nanotechnology*, 17(2) (2021) 109-121.
17. Anu, Thakur, N., Kumar, K., Sharma, K. K., "Application of Co-doped copper oxide nanoparticles against different multidrug resistance bacteria", *Inorganic and Nano-Metal Chemistry*, 50(10) (2020) 933-943.
18. Yousef, A., Barakat, N. A., Amna, T., Al-Deyab, S. S., Hassan, M. S., Abdel-Hay, A., Kim, H. Y., "Inactivation of pathogenic Klebsiella pneumoniae by CuO/TiO2 nanofibers: A multifunctional nanomaterial via one-step electrospinning", *Ceramics International*, 38(6) (2012) 4525-4532.
19. Thakur, N., Kumar, K., "Effect of (Ag, Co) co-doping on the structural and antibacterial efficiency of CuO nanoparticles: A rapid microwave assisted method", *Journal of Environmental Chemical Engineering*, 8(4) (2020) 104011.
20. Attiya, H. G., Fendi, W. J., Al-Dulaimy, Z. A., Farooq, A., Mohammed, A. M., "Characterization Synthesis Of Copper Oxide. Nanoparticles Application. A Review", *Journal of Pharmaceutical Negative Results*, (2023) 250-256.
21. Thongbai, P., Yamwong, T., Maensiri, S., "Correlation between giant dielectric response and electrical conductivity of CuO ceramic", *Solid state communications*, 147(9-10) (2008) 385-387.
22. Ansari, M. A., Somdee, P., "Piezoelectric Polymeric Foams as Flexible Energy Harvesters: A Review", *Advanced Energy and Sustainability Research*, 3(9) (2022) 2200063..
23. Oruç, Ç., Altındal, A., "Structural and dielectric properties of CuO nanoparticles", *Ceramics International*, 43(14) (2017) 10708-10714.
24. Mallick, P., Sahu, S., "Structure, microstructure and optical absorption analysis of CuO nanoparticles synthesized by sol-gel route", *Nanoscience and Nanotechnology*, 2(3) (2012) 71-74.
25. Xiang, Q., Yu, J., Wang, W., Jaroniec, M., "Nitrogen self-doped nanosized TiO 2 sheets with exposed {001} facets for enhanced visible-light photocatalytic activity", *Chemical Communications*, 47(24) (2011) 6906-6908.
26. Li, D., Leung, Y. H., Djurišić, A. B., Liu, Z. T., Xie, M. H., Gao, J., Chan, W. K., "CuO nanostructures prepared by a chemical method", *Journal of crystal growth*, 282(1-2) (2005) 105-111.
27. Faisal, M., Khan, S. B., Rahman, M. M., Jamal, A., Umar, A., "Ethanol chemi-sensor: Evaluation of structural, optical and sensing properties of CuO nanosheets", *Materials Letters*, 65(9) (2011) 1400-1403.
28. Salavati-Niasari, M., Davar, F., "Synthesis of copper and copper (I) oxide nanoparticles by thermal decomposition of a new precursor", *Materials Letters*, 63(3-4) (2009) 441-443.

29. Vijaya Kumar, R., Elgamiel, R., Diamant, Y., Gedanken, A., Norwig, J., "Sonochemical preparation and characterization of nanocrystalline copper oxide embedded in poly (vinyl alcohol) and its effect on crystal growth of copper oxide", *Langmuir*, 17(5) (2001) 1406-1410.
30. Wang, H., Xu, J. Z., Zhu, J. J., Chen, H. Y., "Preparation of CuO nanoparticles by microwave irradiation", *Journal of crystal growth*, 244(1) (2002) 88-94.
31. Ansari, M. A., Jahan, N., "Structural and Optical Properties of BaO Nanoparticles Synthesized by Facile Co-precipitation Method", *Materials Highlights*, 2(1-2) (2021) 23-28.
32. Wu, R., Ma, Z., Gu, Z., Yang, Y., "Preparation and characterization of CuO nanoparticles with different morphology through a simple quick-precipitation method in DMAC–water mixed solvent", *Journal of Alloys and Compounds*, 504(1) (2010) 45-49.
33. Joseph, D. P., Venkateswaran, C., Sambasivam, S., Choi, B. C., "Effect of Fe alloying on the structural, optical, electrical and magnetic properties of spray-deposited CuO thin films", *Journal of the Korean Physical Society*, 61(3) (2012) 449-454.
34. Thakur, N., Kumar, K., Thakur, V. K., Soni, S., Kumar, A., Samant, S. S., "Antibacterial and photocatalytic activity of undoped and (Ag, Fe) co-doped CuO nanoparticles via microwave-assisted method", *Nanofabrication*, 7 (2022) 62-88.
35. Manna, S., De, S. K., "Room temperature ferromagnetism in Fe doped CuO nanorods", *Journal of magnetism and magnetic materials*, 322(18) (2010) 2749-2753.
36. Meneses, C. T., Duque, J. G. S., Vivas, L. G., Knobel, M., "Synthesis and characterization of TM-doped CuO (TM= Fe, Ni)", *Journal of Non-Crystalline Solids*, 354(42-44) (2008) 4830-4832.
37. Rao, G. N., Yao, Y. D., Chen, J. W., "Influence of Mn substitution on microstructure and magnetic properties of Cu 1− x Mn x O nanoparticles", *Journal of applied physics*, 101(9) (2007) 09H119.
38. Gülen, Y., Bayansal, F., Şahin, B., Cetinkara, H. A., Güder, H. S., "Fabrication and characterization of Mn-doped CuO thin films by the SILAR method", *Ceramics International*, 39(6) (2013) 6475-6480.
39. Thakur, N., Kumar, K., Kumar, A., "Effect of (Ag, Zn) co-doping on structural, optical and bactericidal properties of CuO nanoparticles synthesized by a microwave-assisted method", *Dalton Transactions*, 50(18) (2021) 6188-6203.
40. Basith, N. M., Vijaya, J. J., Kennedy, L. J., Bououdina, M., "Structural, morphological, optical, and magnetic properties of Ni-doped CuO nanostructures prepared by a rapid microwave combustion method", *Materials science in semiconductor processing*, 17 (2014) 110-118
41. Al-Amri, S., Shahnawaze A, M., Rafique, S., Aldhahri, M., Rahimuddin, S., Azam, A., Memic, A., "Ni doped CuO nanoparticles: structural and optical characterizations", *Current Nanoscience*, 11(2) (2015) 191-197.
42. Lakshmi, K., Kadirvelu, K., Mohan, P. S., "Catalytic reduction of hazardous compound (Triethylphosphate) using Ni doped CuO nanoparticles", *Defence Life Science Journal*, (2) (2017) 4.
43. Thangamani, C., Ponnar, M., Priyadharshini, P., Monisha, P., Gomathi, S. S., Pushpanathan, K., "Magnetic behavior of ni-doped cuo nanoparticles synthesized by microwave irradiation method", *Surface Review and Letters*, 26(05) (2019) 1850184.
44. Arunachalam, P., Nagarani, S., Prasad, S., AlSalhi, M. S., Al-Mayouf, A. M., Moydeen, M., Ganapathy, S., "Facile coprecipitation synthesis of nickel doped copper oxide nanocomposite as electrocatalyst for methanol electrooxidation in alkaline solution", *Materials Research Express*, *5*(1) (2018) 015512.
45. Brown, I. W. M., Mackenzie, K. J. D., Gainsford, G. J., "Thermal decomposition of the basic copper carbonates malachite and azurite", *Thermochimica acta*, 75(1-2) (1984) 23-32.
46. Karthikeyan, B., "Raman spectral probed electron–phonon coupling and phonon lifetime properties of Ni-doped CuO nanoparticles", *Applied Physics A*, 127(3) (2021) 1-7.
47. Holzwarth, U., Gibson, N., "The Scherrer equation versus the'Debye-Scherrer equation"', *Nature nanotechnology*, 6(9) (2011) 534-534.
48. Ho, W. C. J., Tay, Q., Qi, H., Huang, Z., Li, J., Chen, Z., "Photocatalytic and adsorption performances of faceted cuprous oxide (Cu2O) particles for the removal of methyl orange (MO) from aqueous media", *Molecules*, 22(4) (2017) 677.
49. Zhang, Y.C., Tang, J.Y., Wang, G.L., Zhang, M., Hu, X.Y., "Facile synthesis of submicron Cu2O and CuO crystallites from a solid metallorganic molecular precursor", *J. Cryst. Growth*, 294(2) (2006) 278-282.
50. Tauc, J., "Optical properties and electronic structure of amorphous semiconductors", *Optical Properties of Solids*, (1969) 123-136.
51. Borgohain, K., Singh, J. B., Rao, M. R., Shripathi, T., Mahamuni, S., "Quantum size effects in CuO nanoparticles", *Physical Review B*, 61(16) (2000) 11093.
52. Son, D. I., You, C. H., Kim, T. W., "Structural, optical, and electronic properties of colloidal CuO nanoparticles formed by using a colloid-thermal synthesis process", *Appl. Surf. Sci.*, 255(21) (2009) 8794-8797.

53. Chandrasekar, M., Subash, M., Logambal, S., Udhayakumar, G., Uthrakumar, R., Inmozhi, C., Kanimozhi, K. “Synthesis and characterization studies of pure and Ni doped CuO nanoparticles by hydrothermal method”, *Journal of King Saud University-Science*, (2022) 101831.
54. Govindaraj, G., “Novel Concept of Non-Debye Dipole Relaxation Processes for the Interpretation of Physical Origin of Dielectric Loss in the Glass Formers, Drugs, Polymers and Plastic Crystals”, *arXiv preprint* (2016) arXiv:1608.05304.
55. Sagadevan, S., Priya, M., “Electrical properties of copper oxide nanoparticles”, *Journal of Nano Research*, 30 (2015) 1-8.